International Journal of Thermal Sciences 222 (2026) 110556

Contents lists available at ScienceDirect

International Journal of Thermal Sciences

journal homepage: www.elsevier.com/locate/ijts

Mixed convection and onset of instability due to asymmetric wall heat fluxes in a porous channel

A. Barletta *, M. Celli, P.V. Brandão

Department of Industrial Engineering, Alma Mater Studiorum Università di Bologna, Viale Risorgimento 2, 40136 Bologna, Italy

ARTICLE INFO

Keywords:
Mixed convection
Porous medium
Wall heat flux
Linear instability
Normal modes
Rayleigh number

ABSTRACT

The problem of convective instability onset in a horizontal porous channel is explored. The channel's impermeable walls are heated with asymmetric thermal conditions modelled through unequal, but uniform, wall heat fluxes. A stationary solution describing the mixed convection flow is obtained from the governing local balance equations. Then, the linear instability of this flow is analysed by formulating an eigenvalue problem with normal modes. The research specifically highlights the role of the flow rate regime, parametrised through the Péclet number, where the Rayleigh number and the heat flux asymmetry ratio are key to defining when instability occurs. The numerical solution of the stability eigenvalue problem is achieved by employing the shooting method. Analytical results are also obtained by employing large-wavelength asymptotic expansions. A numerical analysis is performed to discuss the neutral stability curves and the critical values of the Rayleigh number under different flow and asymmetry conditions.

1. Introduction

The study of mixed convection in porous media obtained considerable attention within the thermal science community due to its critical importance in a wide range of engineering and geophysical applications, such as compact heat exchangers, geothermal energy extraction, nuclear waste disposal, building insulation, and subsurface contaminant transport. Mixed convection arises when free convection, governed by the buoyancy force, occurs with an underlying forced flow induced by an externally imposed pressure gradient. The complex interaction between these two modes of heat transfer displays peculiar features in porous media, where the presence of a solid matrix introduces additional resistance to flow and alters the effective thermal diffusivity of the system.

In practical scenarios, porous channels are frequently subject to uniform heat flux boundary conditions [1], either due to operational constraints or environmental factors. Such configurations may involve asymmetric wall heat fluxes, where the two confining walls of a porous channel are subjected to unequal thermal input. The resulting velocity and temperature fields reflect the complexity of the flow dynamics, particularly in the transition to buoyancy-induced instability.

The onset of instability in mixed convection flows through porous channels has been studied under various boundary conditions and flow regimes [2–14], but the influence of asymmetric wall heat fluxes remains an area that is relatively less explored. An exception is the paper by Sphaier and Barletta [10] which, however, focusses on a quite special configuration with uniform heating from the lower boundary and an adiabatic upper boundary. Instability in such systems can manifest as travelling modes depending on the Péclet number. These phenomena not only affect the overall heat transfer performance, but also have implications for system control and stability in real-world applications.

When analysing stability, linear theory is often employed to determine the neutral stability condition and the critical thresholds at which the base flow becomes unstable to small-scale perturbations [1,15,16]. The governing local balance equations are linearised with perturbations superposed to the steady-state base solution. In the context of a parallel-plate porous channel with asymmetric wall heat fluxes, the base temperature field displays a gradient inclined to the vertical. This, in turn, may result in an unstably stratified fluid density distribution in the vertical direction potentially destabilising the mixed convection flow due to the effect of buoyancy. The degree of wall heat flux asymmetry, characterised by a wall heating ratio, plays a crucial role in modulating the threshold for the onset of the instability.

This study aims to provide a comprehensive analysis of mixed convection and the onset of instability in a horizontal porous channel subject to asymmetric wall heat fluxes. In this approach, the study carried out in this paper provides a development of the analyses presented in Barletta [8] and in Barletta et al. [9,13], by relaxing

* Corresponding author.
E-mail address: antonio.barletta@unibo.it (A. Barletta).

https://doi.org/10.1016/j.ijthermalsci.2025.110556
Received 28 August 2025; Received in revised form 7 November 2025; Accepted 30 November 2025
Available online 4 December 2025

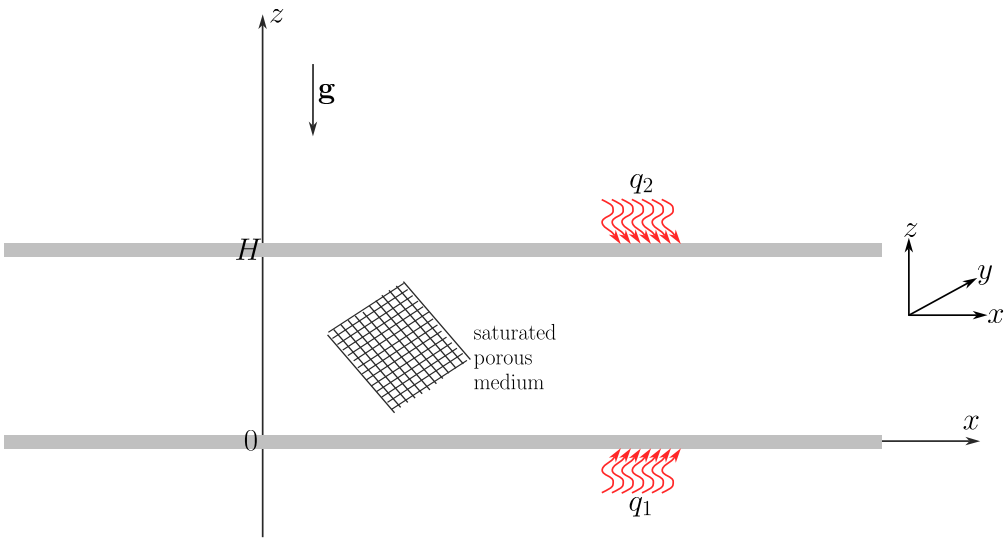

Fig. 1. A drawing of the porous channel.

the symmetry assumption in the temperature boundary conditions. Furthermore, the very special asymmetric case (uniform heating from the lower boundary with an adiabatic upper boundary) investigated by Sphaier and Barletta [10] is generalised in the forthcoming analysis. By systematically varying the governing parameters, including the dimensionless streamwise temperature gradient, the Rayleigh number and the asymmetry ratio, the conditions leading to the loss of flow stability are identified. The critical thresholds for convective instability are determined using linear stability analysis, and the influence of wall heat flux asymmetry on the structure and nature of the unstable modes is accounted for. The results offer valuable insights into the fundamental mechanisms that drive instability in porous media under non-symmetric thermal boundary conditions, with implications for the design and optimisation of thermal systems involving porous structures. An example of such applications is the heat transfer enhancement obtained by using metal foams for the design of innovative heat exchangers [17,18].

2. Model description

We aim to analyse the buoyant flow in a horizontal porous channel saturated by a fluid. The channel height is H and its width in both the horizontal directions x and y is infinite. The channel impermeable walls, $z = 0$ and $z = H$, are either heated or cooled by asymmetric and uniform heat fluxes, q_1 and q_2, which can be positive (incoming flux) or negative (outgoing flux). Fig. 1 shows a sketch of the porous channel and of its net wall heating/cooling conditions.

2.1. Experimental evidence

The emergence of secondary buoyancy-induced flow for a parallel velocity field in a horizontal channel subject to uniform heat flux boundary conditions has been documented experimentally by many authors [19–22]. As pointed out by Lin and Lin [19], when "the heat flux is increased beyond certain critical value depending on Re, the Nusselt number exhibits a discernible departure from the forced convection limit indicating the onset of the longitudinal vortex rolls". Here, Re denotes the Reynolds number and the critical value of the heat flux, in fact, implies a critical Rayleigh number associated with the underlying forced flow. The onset of vortex rolls is mathematically meant to denote flow instability, caused by the thermal buoyancy. Although conceptually different from the hydrodynamic instability involved in the Orr–Sommerfeld problem [23,24], the buoyancy-induced type of instability causing the secondary flow in mixed convection is analysed via the same mathematical scheme. In particular, the Oberbeck-Boussinesq approximation [25,26] is employed and the critical value of the Rayleigh number is predicted by a linear analysis of flow instability. In other words, the secondary flow is assumed to be caused by the unavoidable and random disturbance of arbitrarily small amplitude acting on the forced flow and perturbing its structure.

If the experimental study of buoyancy-induced instability is mainly focussed on fluids clear of solid material, there are a few papers showing up similar phenomena in porous media saturated by a fluid [27–29]. Kurtbas and Celik [29] investigated flow in a rectangular channel where all the boundaries are uniformly heated. Open-cell metal foams saturated by air were employed. The onset of secondary flow is monitored by testing the change of the Nusselt number describing the heat transfer at the bounding walls. These authors pointed out that "buoyancy driven secondary flow has an important effect on the Nusselt number from the inlet to the middle of the channel for each pore density".

The above mentioned experimental studies show the importance of predicting the parametric conditions for the initiation of instability in an underlying parallel flow. Such conditions can be established quite accurately starting from a proper mathematical model of the buoyant flow in a porous medium.

2.2. Governing equations

The buoyant flow in the porous medium is modelled by employing Darcy's law [1] and the Oberbeck-Boussinesq approximation [25,26]. In this framework, the local balance equations for mass, momentum and energy are given by

$$\begin{aligned} &\boldsymbol{\nabla}\cdot\mathbf{u} = 0,\\ &\frac{\mu}{K}\mathbf{u} = -\boldsymbol{\nabla}p - \rho_0\,\beta(T - T_0)\mathbf{g},\\ &\rho_0\,c\left(\xi\frac{\partial T}{\partial t} + \mathbf{u}\cdot\boldsymbol{\nabla}T\right) = \chi\nabla^2 T, \end{aligned} \tag{1}$$

while the boundary conditions are written as

$$\begin{aligned} &z = 0: \qquad w = 0, \quad -\chi\frac{\partial T}{\partial z} = q_1,\\ &z = H: \qquad w = 0, \quad \chi\frac{\partial T}{\partial z} = q_2. \end{aligned} \tag{2}$$

Here, $\mathbf{u}$ is the seepage velocity with Cartesian components (u, v, w), p is the local difference between the pressure and the hydrostatic pressure, T is the temperature, t is the time, (x, y, z) are the Cartesian coordinates.

Furthermore, ρ_0 is the fluid density evaluated at the reference temperature T_0, μ is the dynamic viscosity of the fluid, K is the permeability of the porous medium, β is the thermal expansion coefficient of the fluid, c is the specific heat capacity of the fluid, ξ is the ratio between the average volumetric heat capacity of the porous medium and the volumetric heat capacity of the fluid, while χ is the effective thermal conductivity of the porous medium evaluated as the average value of the conductivities for the solid and fluid phases weighted by the porosity. The gravitational acceleration is expressed by $\mathbf{g} = -g\,\mathbf{e}_z$, where g is its modulus. The unit vectors along the (x, y, z) axes are denoted by $(\mathbf{e}_x, \mathbf{e}_y, \mathbf{e}_z)$.

2.3. Dimensionless formulation

The governing equations can be rewritten in a non-dimensional form by means of the scaling

$$\frac{(x,y,z)}{H} \to (x,y,z), \quad \frac{\chi}{\rho_0\, c\, H^2 \xi}\, t \to t, \quad \frac{\rho_0\, c\, H}{\chi}\,\mathbf{u} \to \mathbf{u}, \quad \frac{\rho_0\, c\, K}{\chi\, \mu}\, p \to p,$$
$$\frac{T - T_0}{\Delta T} \to T, \quad \text{for} \quad \Delta T = \frac{\chi\, \mu}{\rho_0^2\, c\, \beta\, g\, K\, H}. \tag{3}$$

Thus, Eqs. (1) and (2) can be expressed as

$$\begin{aligned} &\boldsymbol{\nabla}\cdot\mathbf{u} = 0,\\ &\mathbf{u} = -\boldsymbol{\nabla} p + T\,\mathbf{e}_z,\\ &\frac{\partial T}{\partial t} + \mathbf{u}\cdot\boldsymbol{\nabla} T = \nabla^2 T,\\ &z = 0: \quad w = 0, \quad \frac{\partial T}{\partial z} = -Ra,\\ &z = 1: \quad w = 0, \quad \frac{\partial T}{\partial z} = \sigma\, Ra, \end{aligned} \tag{4}$$

where Ra is the Darcy–Rayleigh number associated with the heat flux q_1 and σ is the flux asymmetry ratio,

$$Ra = \frac{\rho_0^2\, c\, \beta\, g\, K\, H^2 q_1}{\chi^2 \mu}, \quad \sigma = \frac{q_2}{q_1}. \tag{5}$$

Since q_1 and q_2 might be either positive or negative, both the Rayleigh number Ra and the asymmetry ratio σ can assume a positive or a negative value, accordingly.

2.4. Basic state

A stationary flow solution of (4) defines the basic state,

$$\begin{aligned} &\mathbf{u}_b = \left[Pe + \gamma\left(\frac{1}{2} - z\right)\right](\cos\varphi\,\mathbf{e}_x + \sin\varphi\,\mathbf{e}_y),\\ &\boldsymbol{\nabla} T_b = \gamma\,(\cos\varphi\,\mathbf{e}_x + \sin\varphi\,\mathbf{e}_y) + \left\{Ra\,[(1+\sigma)z - 1] + \frac{\gamma^2}{2}\,z\,(1-z)\right\}\mathbf{e}_z,\\ &\boldsymbol{\nabla} p_b = (-u_b, -v_b, T_b), \end{aligned} \tag{6}$$

where

$$\gamma = \frac{Ra(1+\sigma)}{Pe}, \tag{7}$$

while the symbol Pe denotes the Péclet number relative to the mean flow rate. Thus, the dimensionless mean velocity along the basic flow direction is given by

$$Pe = \int_0^1 \mathbf{u}_b\cdot\mathbf{n}\,\mathrm{d}z, \quad \text{for} \quad \mathbf{n} = \cos\varphi\,\mathbf{e}_x + \sin\varphi\,\mathbf{e}_y. \tag{8}$$

A horizontal parallel flow along the $\mathbf{n}$ direction is implied by (6) and (8). A singularity affects such a flow for $Pe \to 0$, with the only exception of the special case $\sigma = -1$. In fact, a steady-state flow is allowed only if a net positive or negative heat flux is supplied through the boundaries $z = 0, 1$ that is convected downstream by the fluid flow or, alternatively, if the net heat flux supplied is zero ($\sigma = -1$). We mention that this basic state is exactly the same as that considered by Barletta [8] relative to the symmetric special case $\sigma = 1$. On the other hand, the special case $\sigma = -1$ is equivalent to the isoflux-isoflux Horton-Rogers-Lapwood problem contemplated in Table 6.1 of the book by Nield and Bejan [1]. We note that the analysis of the latter problem has been recently generalised by Brandão et al. [30] and by Turkyilmazoglu and Siddiqui [31].

One can easily check that (6) describes a flow state where the vertical component of the temperature gradient can be negative for some ranges of z, thus yielding conditions of possibly unstable density stratification. Where and how such ranges of z are localised depend on the three governing parameters (Ra, Pe, σ). In fact, a negative $\partial T_b/\partial z$ occurs when

$$\frac{\gamma^2}{2}\,z\,(1-z), \tag{9}$$

is smaller than

$$Ra[1 - (1+\sigma)z]. \tag{10}$$

Such a condition may happen for some subset of the interval $0 \le z \le 1$ depending solely on the values of (Ra, σ). Fig. 2 shows qualitatively how the signs of Ra and σ may determine the existence of regions of possibly unstable density stratification, where $\partial T_b/\partial z < 0$. If the existence of regions where $\partial T_b/\partial z < 0$ is determined just by the signs of Ra and σ (see Fig. 3), the value of the parameter γ influences the width of such regions.

Whether a possibly unstable density stratification may yield an actual linear instability can be decided by investigating the dynamics of small perturbations acting on the basic flow state.

3. Linear instability

The basic flow state (6) occurs along a direction $\mathbf{n}$ inclined an angle φ with respect to the x axis. This seemingly useless complication in the mathematics turns out to be, on the contrary, a simplification when the linear stability analysis is formulated. In fact, the general oblique modes of perturbation can be identified by the y independent modes propagating along the x axis. Their directional effect is then easily spanned by letting φ vary in the range $[0, \pi/2]$ where, actually, $\varphi = 0$ means transverse modes and $\varphi = \pi/2$ longitudinal modes.

3.1. Streamfunction-temperature formulation

As already pointed out, the analysis of the onset of linear instability is formulated by employing y independent normal modes, that can be conveniently expressed through a streamfunction, ψ, namely

$$\begin{aligned} &u(x,y,z,t) = u_b(z) + \varepsilon\,\frac{\partial\psi(x,z,t)}{\partial z}, \quad v(x,y,z,t) = v_b(z) + \varepsilon\, V(x,z,t),\\ &w(x,y,z,t) = -\varepsilon\,\frac{\partial\psi(x,z,t)}{\partial x}, \quad T(x,y,z,t) = T_b(x,y,z) + \varepsilon\,\theta(x,z,t), \end{aligned} \tag{11}$$

with ε the small perturbation parameter ($|\varepsilon| \ll 1$) and (ψ, V, θ) the perturbation fields. As a consequence of the streamfunction definition, the local mass balance equation, namely the first Eq. (4), becomes an identity. Furthermore, the y component of the local momentum balance, given by the second Eq. (4), yields $V(x,z,t) = 0$. Eventually, the substitution of (11) into (4) yields, to $\mathcal{O}(\varepsilon)$, the linear partial differential equations and boundary conditions for the perturbation fields, with a (ψ, θ) formulation,

$$\begin{aligned} &\frac{\partial^2\psi}{\partial x^2} + \frac{\partial^2\psi}{\partial z^2} + \frac{\partial\theta}{\partial x} = 0,\\ &\frac{\partial\theta}{\partial t} + \frac{\partial T_b}{\partial x}\frac{\partial\psi}{\partial z} - \frac{\partial T_b}{\partial z}\frac{\partial\psi}{\partial x} + u_b\frac{\partial\theta}{\partial x} = \frac{\partial^2\theta}{\partial x^2} + \frac{\partial^2\theta}{\partial z^2},\\ &z = 0, 1: \quad \psi = 0, \quad \frac{\partial\theta}{\partial z} = 0. \end{aligned} \tag{12}$$

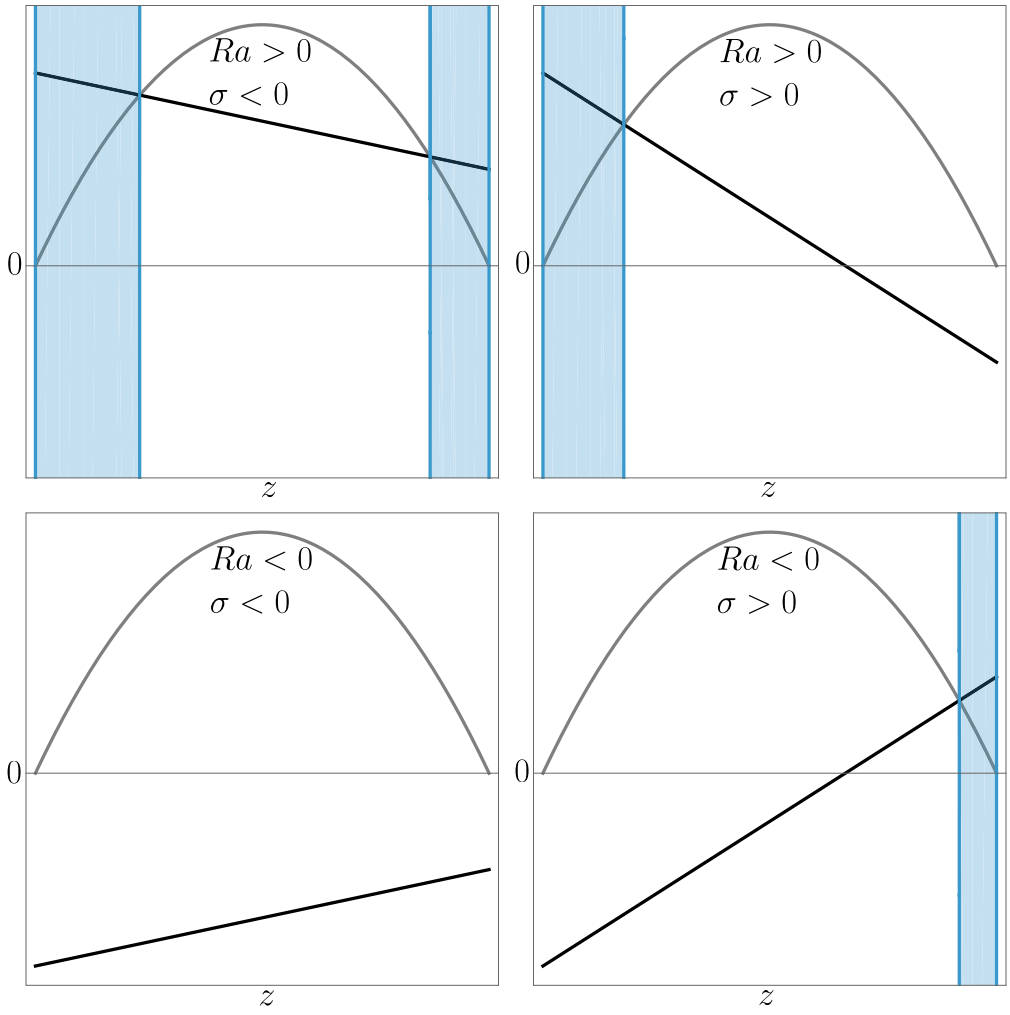

Fig. 2. Qualitative plots of the functions of z given by (9) (grey line) and (10) (black line); the blue regions denote $\partial T_b/\partial z < 0$.

3.2. Fourier normal modes

The perturbation fields (ψ, θ) are now written as Fourier normal modes with wavenumber k, time growth rate η and angular frequency ω,

$$\psi(x,z,t) = i\, f(z)\, e^{i\,(kx-\omega\, t)}\, e^{\eta\, t}, \qquad \theta(x,z,t) = h(z)\, e^{i\,(kx-\omega\, t)}\, e^{\eta\, t}, \tag{13}$$

where $f(z)$ and $h(z)$ represent the eigenfunctions for the instability eigenvalue problem, formulated by substituting (13) into (12),

$$\begin{aligned} &f'' - k^2\, f + k\, h = 0, \\ &h'' - \left[k^2 + i\, k \left(\frac{1}{2} - z\right) \gamma\, \cos\varphi + \eta - i\, \tilde{\omega}\right] h \\ &\quad - i\, \gamma\, \cos\varphi\, f' - k \left\{ Ra\, [(1+\sigma)z - 1] + \frac{\gamma^2}{2}\, z\,(1-z) \right\} f = 0, \\ &z = 0, 1: \qquad f = 0, \quad h' = 0, \end{aligned} \tag{14}$$

where

$$\tilde{\omega} = \omega - k\, Pe\, \cos\varphi, \tag{15}$$

is the reduced angular frequency.

We note that the eigenvalue problem (14) depends on the perturbation characteristic parameters $(k, \eta, \tilde{\omega})$ and on the flow governing parameters $(Ra, \sigma, \gamma, \varphi)$. If the general case $0 < \varphi < \pi/2$ identifies the oblique modes, the limiting cases $\varphi = 0$ and $\varphi = \pi/2$ define the transverse modes and the longitudinal modes, respectively.

We point out that the eigenvalue problem (14) loses any explicit dependence on the angle φ in the special case where $\gamma \to 0$. This means that, in the limit $\gamma \to 0$, all perturbations ranging from longitudinal to transverse are equivalent in defining the threshold to linear instability. The physical meaning of such a limiting case, for nonzero Ra and $\sigma \neq -1$, is that of an infinitely large Péclet number, as one can easily reckon from (7). This, in turn, means an extremely large horizontal throughflow across the porous medium or, equivalently, an extremely efficient streamwise convection of the unbalanced wall heat fluxes. As a matter of fact, an independence of the linear instability condition on both Pe and φ is exactly what happens also when $\sigma = -1$ (balanced wall heat fluxes), namely, for the isoflux-isoflux Horton-Rogers-Lapwood problem [1] that, again, means $\gamma = 0$ whatever are the values of Ra and Pe.

The numerical solution of (14) is achieved for input parameters $(k, \sigma, \gamma, \eta, \varphi)$ by determining the eigenvalue pair $(Ra, \tilde{\omega})$. In particular, the numerical determination of the neutral stability threshold is achieved by setting $\eta = 0$. For fixed $(\sigma, \gamma, \varphi)$, the minimum of Ra among the neutral stability values for all possible k is the critical Rayleigh number, Ra_c, while the corresponding k is the critical wavenumber, k_c. The shooting method is employed, according to the general guidelines provided in Chapter 19 of Straughan [15] or in Chapter 10 of Barletta [16]. The software environment *Wolfram 14* (© Wolfram Research, Inc.) [32] provides the fundamental tool for the coding of the solution method, with function `NDSolve` as the numerical solver of the initial value problem starting from $z = 0$ and function `FindRoot` for the determination of the parameters fitting the target conditions at $z = 1$.

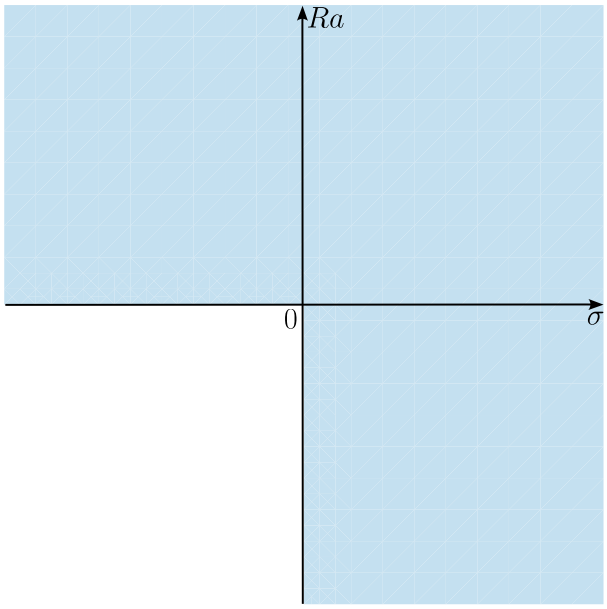

Fig. 3. Unstable density stratification: the blue region denotes the parametric conditions for the existence of ranges of z where $\partial T_b/\partial z < 0$.

3.3. Testing the numerical code with experimental data

A test of the numerical accuracy can be carried out by considering the special case where $\sigma = -1$, which implies $\gamma = 0$ according to (7). In this case, we can obtain the traditional Horton-Rogers-Lapwood problem [1] by replacing the isoflux boundary conditions declared in (14) with isothermal boundary conditions, namely by replacing the last line of (14) with

$$z = 0, 1: \qquad f = 0, \quad h = 0. \tag{16}$$

In fact, the numerical solution for this special case yields the critical values

$$k_c = 3.1415926535897752, \quad Ra_c = 39.4784176043569820, \tag{17}$$

while the exact analytical solution for the same case leads to [1]

$$k_c = \pi, \quad Ra_c = 4\pi^2, \tag{18}$$

with a relative error given by

$$|\Delta k_c|/k_c = 6 \times 10^{-15}, \quad |\Delta Ra_c|/Ra_c = 1 \times 10^{-14}. \tag{19}$$

This tuning of the model facilitates the comparison with experiments. One can, in particular, consider the experimental tests for the Horton-Rogers-Lapwood problem carried out by Buretta and Berman [33]. These authors employed porous layers made up of packed glass beads saturated by demineralised water. They observed that [33]: "one obtains 38.0 as an estimate of the critical Rayleigh number at which the energy transfer mechanism changes from conduction to convection. This is in good agreement with the prediction of $4\pi^2 (= 39.48)$ obtained from earlier analytical investigations". The slight theoretical overestimate of Ra_c can be explained by a minor departure from perfectly isothermal bounding walls in the actual experimental system employed by Buretta and Berman [33].

Direct comparison with experimental data for the case where $\sigma \neq -1$ is absent. We acknowledge this limitation and we call for future experimental work to prioritise asymmetric heating conditions where $\sigma \neq -1$, thereby addressing this validation gap.

4. Asymptotic analysis for modes with very large wavelength

We consider the neutral stability condition, *i.e.*, we set $\eta = 0$. We can now express $f(z)$, $h(z)$, Ra and $\tilde{\omega}$ as power series with respect to k by keeping the lowest orders. In other words, we determine the solution for small wavenumbers k, namely for the large wavelength regime. We write

$$\begin{aligned} f(z) &= f_0(z) + f_1(z)k + f_2(z)k^2 + f_3(z)k^3 + \ \dots\ , \\ h(z) &= h_0(z) + h_1(z)k + h_2(z)k^2 + h_3(z)k^3 + \ \dots\ , \\ Ra &= Ra_0 + Ra_1 k + Ra_2 k^2 + Ra_3 k^3 + \ \dots\ , \\ \tilde{\omega} &= \tilde{\omega}_0 + \tilde{\omega}_1 k + \tilde{\omega}_2 k^2 + \tilde{\omega}_3 k^3 + \ \dots\ . \end{aligned} \tag{20}$$

By substituting (20) into (14) and by collecting like powers of k, we obtain to $\mathcal{O}(k^0)$,

$$\begin{aligned} &f_0'' = 0, \qquad \text{for} \quad f_0(0) = 0, \quad f_0(1) = 0, \\ &h_0'' - i\,\gamma\,\cos\varphi\, f_0' + i\,\tilde{\omega}_0\, h_0 = 0, \qquad \text{for} \quad h_0'(0) = 0, \quad h_0'(1) = 0, \end{aligned} \tag{21}$$

where the first (21) yields $f_0(z) = 0$ for $0 \le z \le 1$, while the second (21) yields $\tilde{\omega}_0 = 0$ and $h_0(z) = constant$. Such a constant can be arbitrarily chosen meaning that we can gauge the otherwise arbitrary amplitude of the perturbation. A convenient choice is $h(0) = 1$, so that we can write $h_0(0) = 1$ and $h_n(0) = 0$, for every integer $n > 0$. Thus, we obtain $h_0(z) = 1$ for $0 \le z \le 1$. To $\mathcal{O}(k)$, we get

$$\begin{aligned} &f_1'' + 1 = 0, \qquad \text{for} \quad f_1(0) = 0, \quad f_1(1) = 0, \\ &h_1'' - i\,\gamma\,\cos\varphi\, f_1' - i\left[\left(\frac{1}{2} - z\right)\gamma\,\cos\varphi - \tilde{\omega}_1\right] = 0, \\ &\qquad\qquad \text{for} \quad h_1(0) = 0, \quad h_1'(0) = 0, \quad h_1'(1) = 0, \end{aligned} \tag{22}$$

namely,

$$f_1(z) = \frac{1}{2} z\,(1 - z), \quad h_1(z) = -\frac{iz^2}{6}(2z - 3)\,\gamma\,\cos\varphi, \quad \tilde{\omega}_1 = 0. \tag{23}$$

To $\mathcal{O}(k^2)$, one has

$$\begin{aligned} &f_2'' + h_1 = 0, \qquad \text{for} \quad f_2(0) = 0, \quad f_2(1) = 0, \\ &h_2'' - i\,\gamma\cos\varphi\, f_2' - i\left(\frac{1}{2} - z\right)\gamma\,\cos\varphi\, h_1 \\ &- \left\{ Ra_0\,[(\sigma + 1)\,z - 1] + \frac{\gamma^2}{2}\, z\,(1 - z) \right\} f_1 - 1 + i\,\tilde{\omega}_2 = 0, \\ &\quad \text{for} \quad h_2(0) = 0, \quad h_2'(0) = 0, \quad h_2'(1) = 0. \end{aligned} \tag{24}$$

We do not write here the expressions of $f_2(z)$ and $h_2(z)$ for the sake of brevity. We just say that (24) serves to determine explicitly Ra_0 and $\tilde{\omega}_2$,

$$Ra_0 = \frac{120 + \gamma^2\left(1 + 2\,\cos^2\varphi\right)}{5\,(1 - \sigma)}, \quad \tilde{\omega}_2 = 0. \tag{25}$$

A finite Ra_0 exists for every (γ, σ) except for $\sigma = 1$, which is the special case studied in Barletta [8] and extended to the anisotropic case in Barletta et al. [13]. We also note that $|Ra_0|$ is a monotonic decreasing function of φ, for prescribed (γ, σ), meaning that the lowest neutral stability values of $|Ra|$ in the limit $k \to 0$ are obtained with longitudinal modes ($\varphi = \pi/2$).

One may develop also the $\mathcal{O}(k^3)$ and $\mathcal{O}(k^4)$ differential problems. We mention that the $\mathcal{O}(k^3)$ solution provides the evaluation of Ra_1 and $\tilde{\omega}_3$,

$$Ra_1 = 0, \quad \tilde{\omega}_3 = \frac{(1 + \sigma)\left[120 + \gamma^2\left(1 + 2\,\cos^2\varphi\right)\right]}{6720(1 - \sigma)}\,\gamma\,\cos\varphi. \tag{26}$$

From (26), we understand that oblique and transverse rolls at neutral stability have, in general, a nonzero $\tilde{\omega}$ when $k \neq 0$. As for the $\mathcal{O}(k^4)$ solution, one may get expressions for Ra_2 and $\tilde{\omega}_4$,

$$Ra_2 = -\frac{\gamma^4\left(23\sigma^2 + 42\sigma + 23\right) + 880\,\gamma^2\left(5\sigma^2 + 14\sigma + 5\right)}{2772000(1 - \sigma)^3} + \frac{4(19\sigma^2 - 42\sigma + 19)}{35(1 - \sigma)^3}$$

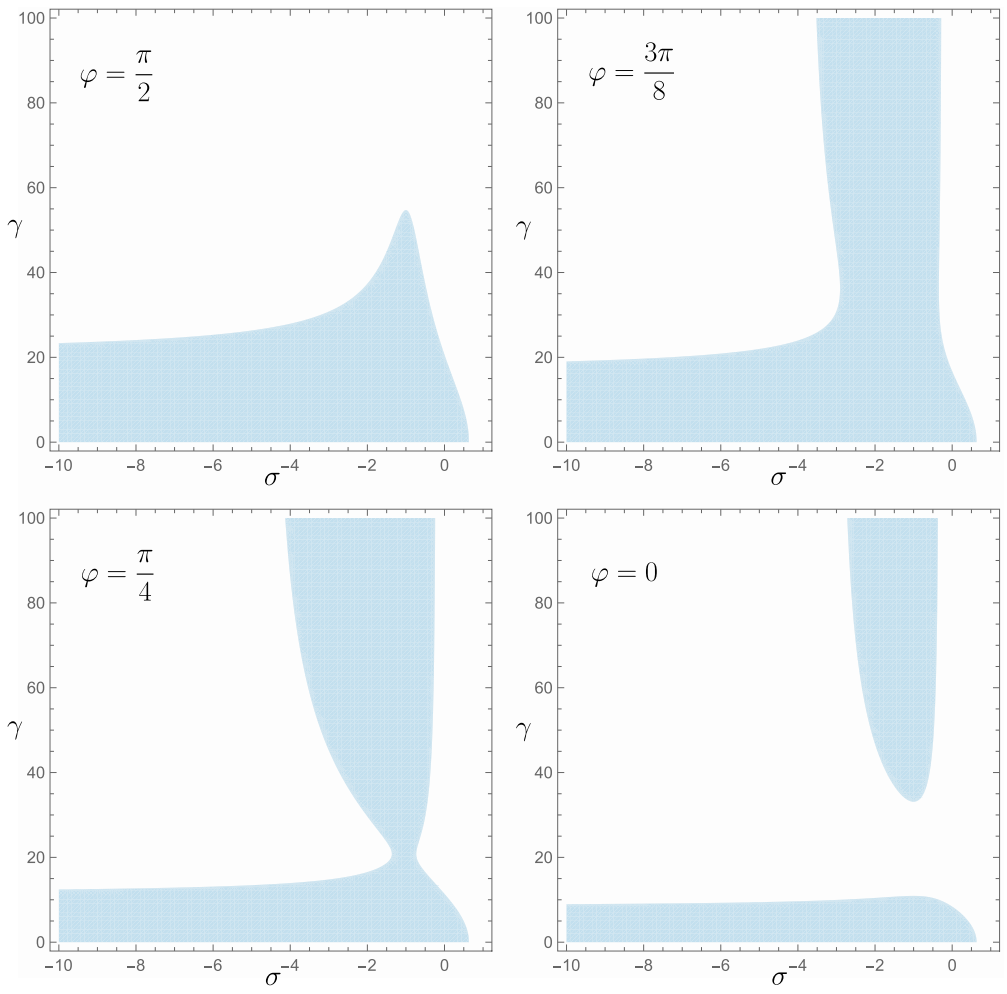

Fig. 4. Regions where $Ra_2 > 0$ (shaded in blue), for $\sigma < 1$ and differently oriented normal modes.

$$-\frac{\gamma^2\left(29\sigma^2+206\sigma+29\right)+7040\left(5\sigma^2-7\sigma+5\right)}{1386000(1-\sigma)^3}\gamma^2\cos^2\varphi$$
$$-\frac{137\sigma^2+78\sigma+137}{5544000(1-\sigma)^3}\gamma^4\cos(2\varphi)\cos^2\varphi, \quad \tilde{\omega}_4 = 0. \tag{27}$$

The sign of Ra_2 is very important in defining whether the neutral stability value of Ra is an increasing or decreasing function of k starting from 0. If $Ra_0 > 0$ and $Ra_2 < 0$, one is sure that the minimum of the neutral stability curve is not achieved with $k \to 0$, but with a critical wave number $k = k_c > 0$. As is well known, the neutral stability value of Ra for $k = k_c$ is termed the critical Rayleigh number and is denoted with Ra_c.

5. Symmetries

On varying the governing parameters (Ra, σ, γ), one can test the conditions for the onset of linear instability. In the determination of the neutral stability curves in the (k, Ra) plane and the evaluation of the critical values $(k_c, Ra_c, \tilde{\omega}_c)$, the analysis is grounded on the mathematical symmetries underlying the eigenvalue problem (14).

The main symmetry displayed by the eigenvalue problem (14) is the invariance of the problem under the transformation

$$z \to 1-z, \quad Ra \to -\sigma Ra, \quad \sigma \to \frac{1}{\sigma}, \quad \gamma \to -\gamma, \quad \varphi \to \varphi,$$
$$k \to k, \quad \eta \to \eta, \quad \tilde{\omega} \to \tilde{\omega}. \tag{28}$$

Such a symmetry justifies the restriction of the parametric domain for the instability analysis to

$$Ra \geq 0, \quad \sigma \in \mathbb{R}, \quad \gamma \in \mathbb{R}, \quad 0 \leq \varphi \leq \frac{\pi}{2}, \tag{29}$$

where $\mathbb{R}$ denotes the set of real numbers. There is a further argument showing that reversing the sign of γ is unimportant as far as $(Ra, \sigma, |\gamma|, \varphi)$ are kept fixed. Indeed, under this condition, a sign change of γ is equivalent to a sign change of Pe, as shown by (7), which means reversing the direction of the basic flow. One can easily conclude that the orientation of the basic flow, $\mathbf{n}$ or $-\mathbf{n}$, is physically insignificant to the instability analysis provided that the inclination of the basic flow streamlines to the x axis, namely the angle φ, remains unaltered. Thus, one can further restrict the parametric domain defined by (29) to

$$Ra \geq 0, \quad \sigma \in \mathbb{R}, \quad \gamma \geq 0, \quad 0 \leq \varphi \leq \frac{\pi}{2}. \tag{30}$$

6. Discussion of the results

By taking $Ra \geq 0$ with a positive or negative σ, the neutral stability curves intersect the positive Ra axis only for $\sigma < 1$, as one can easily infer from (25). For $\sigma \geq 1$, the neutral stability function $Ra(k)$ turns out to be convex having a singularity when $k \to 0$ and a minimum, $Ra = Ra_c > 0$, for $k = k_c > 0$. Regarding the range $\sigma < 1$, the limit $k \to 0$ of the eigenvalue Ra does not yield the critical Rayleigh number, Ra_c, whenever $Ra_2 < 0$. By employing the expression of Ra_2 given by (27), one obtains the plots displayed in Fig. 4 where the shaded regions

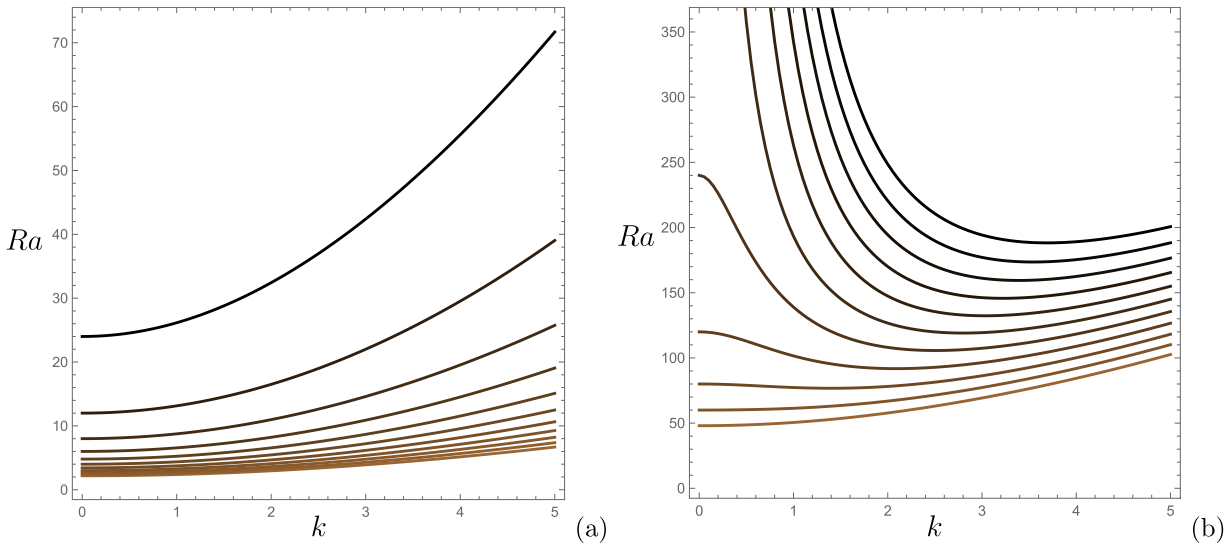

Fig. 5. Limiting case $\gamma \to 0$, neutral stability curves $Ra(k)$ with: (a) σ ranging from -10 to 0 in steps of 1; (b) σ ranging from 0.5 to 1.5 in steps of 0.1. Increasing values of σ are identified with a line colour shifting from brown to black.

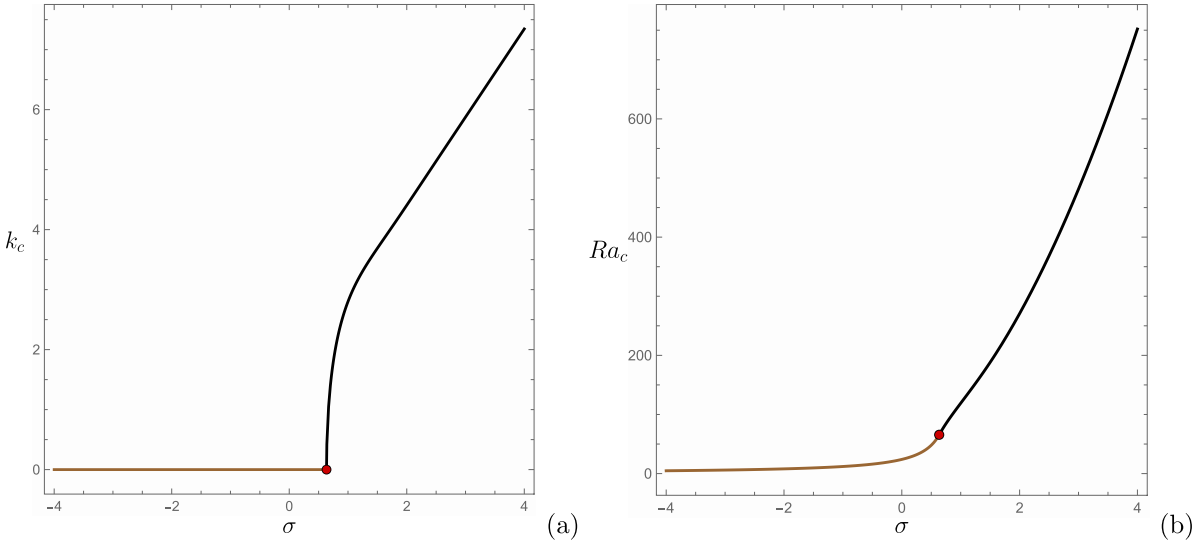

Fig. 6. Limiting case $\gamma \to 0$, Critical values of k (a) and Ra (b) versus σ. The brown lines are relative to the range defined by (31) where $k_c = 0$ and $Ra_c = Ra_0$, while the black lines denote cases where $k_c > 0$.

identify the condition $Ra_2 > 0$.

One may start the exploration from the asymptotic case where the Péclet number is extremely large so that, from (7), one has the $\gamma \to 0$ regime. We also point out that the condition $\gamma = 0$ is the only possible one for $\sigma = -1$, independently of the Péclet number being large or small. This conclusion is an immediate consequence of the definition of γ, given by (7).

6.1. The $\gamma \to 0$ regime

The main feature of the limiting case where $\gamma \to 0$ is the independence of φ for the eigenvalue problem (14). The independence of φ means that every oblique mode is equivalent, in triggering the instability, to transverse and longitudinal modes. This result makes the analysis of this limiting case much simpler than the general case, with the neutral stability curves $Ra(k)$ and the critical values $(k_c, Ra_c, \tilde{\omega}_c)$ depending only on the heat flux ratio σ.

A common feature of the neutral stability curves is that, for every σ and k, the value of $\tilde{\omega}$ is always zero. Furthermore, Fig. 5 shows that the neutral stability curves move upward in the (k, Ra) plane as σ increases. The range explored in this figure is from $\sigma = -10$ to $\sigma = 1.5$. When the neutral stability curve moves upward in the (k, Ra) plane, one has a gradual stabilisation of the basic flow, as the region of linear instability is above the neutral stability curve. Furthermore, one may notice that the neutral stability curves, $Ra(k)$, are monotonic increasing starting from $k = 0$ up to $\sigma = 0.6$. Indeed, the expression of Ra_2 given by (27) ensures that the function $Ra(k)$ at $k = 0$ is convex ($Ra_2 > 0$) provided that

$$\sigma < \frac{1}{19}\left(21 - 4\sqrt{5}\right) \approx 0.634512. \tag{31}$$

When the inequality (31) is not satisfied, then the neutral stability function $Ra(k)$ initially decreases starting from $k = 0$, reaches a minimum for $k = k_c > 0$ and eventually starts increasing. This behaviour is evident in frame (b) of Fig. 5 for the plots with $0.7 \le \sigma \le 0.9$. All the neutral stability curves with $\sigma \ge 1$ display a singularity at $k = 0$ and a minimum $Ra = Ra_c$, for $k = k_c$, which increases with σ.

Fig. 6 shows the plots of the critical values of k and Ra versus σ with the brown colour line identifying the case where the onset of

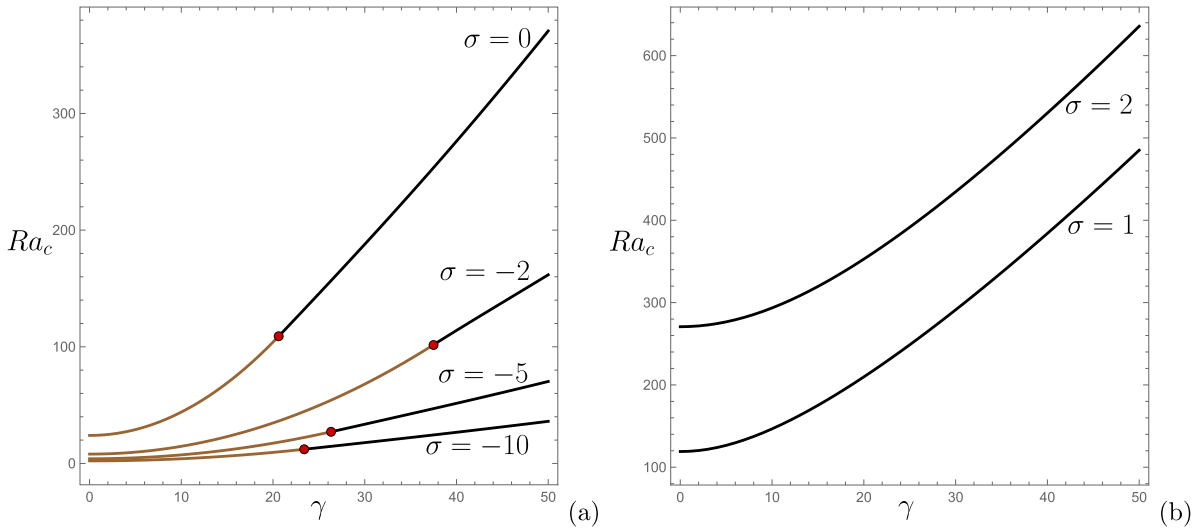

Fig. 7. Critical values of Ra versus γ for different values of $\sigma \leq 0$ (a) or $\sigma > 0$ (b), relative to the longitudinal modes ($\varphi = \pi/2$). The brown lines are for the range where $k_c = 0$ and $Ra_c = Ra_0$, while the black lines denote cases where $k_c > 0$.

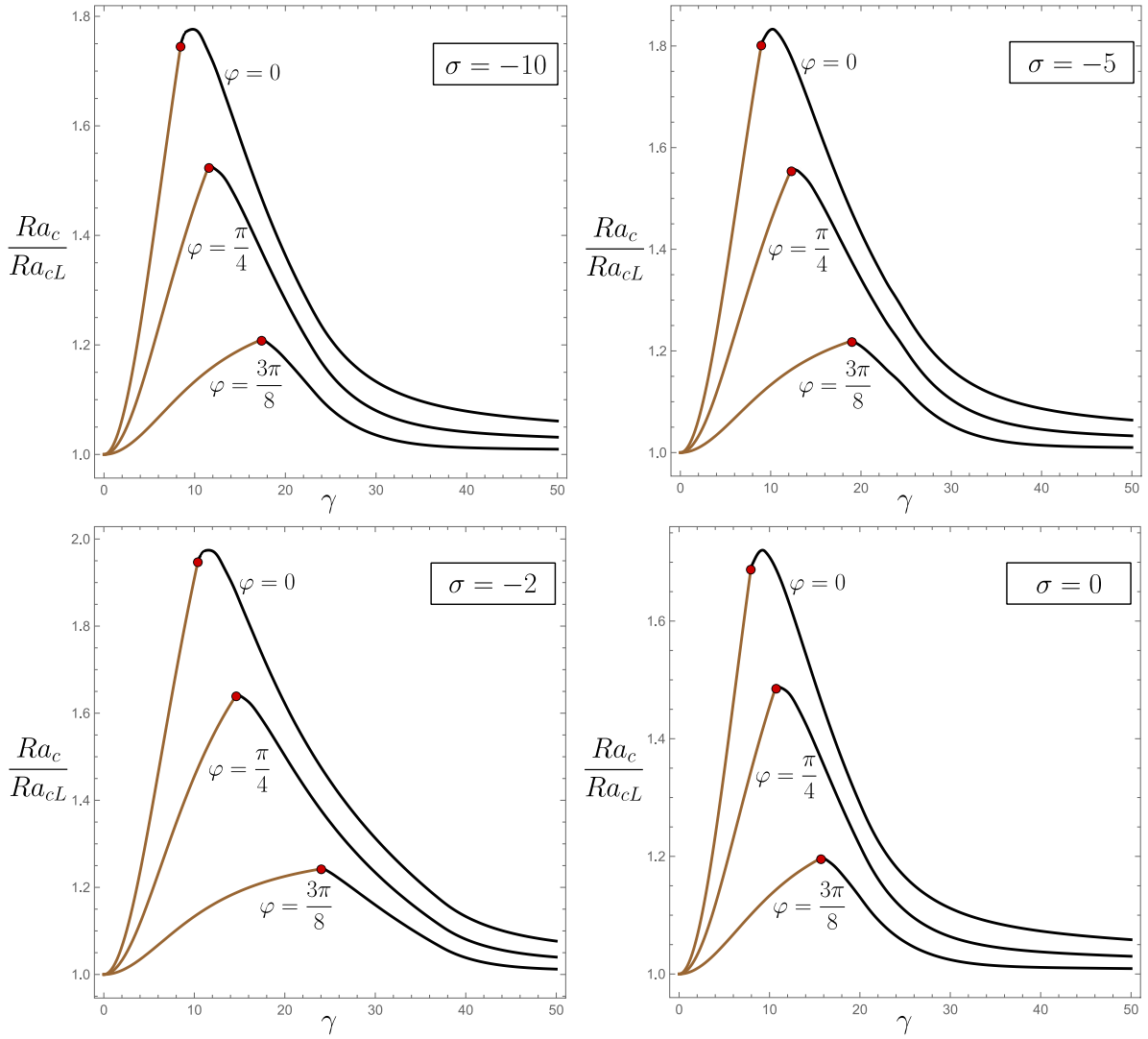

Fig. 8. Ratio between the critical values of Ra evaluated for oblique or transverse modes and those for longitudinal (L) modes versus γ for different values of $\sigma \leq 0$. The brown lines are for the range where $k_c = 0$ and $Ra_c = Ra_0$.

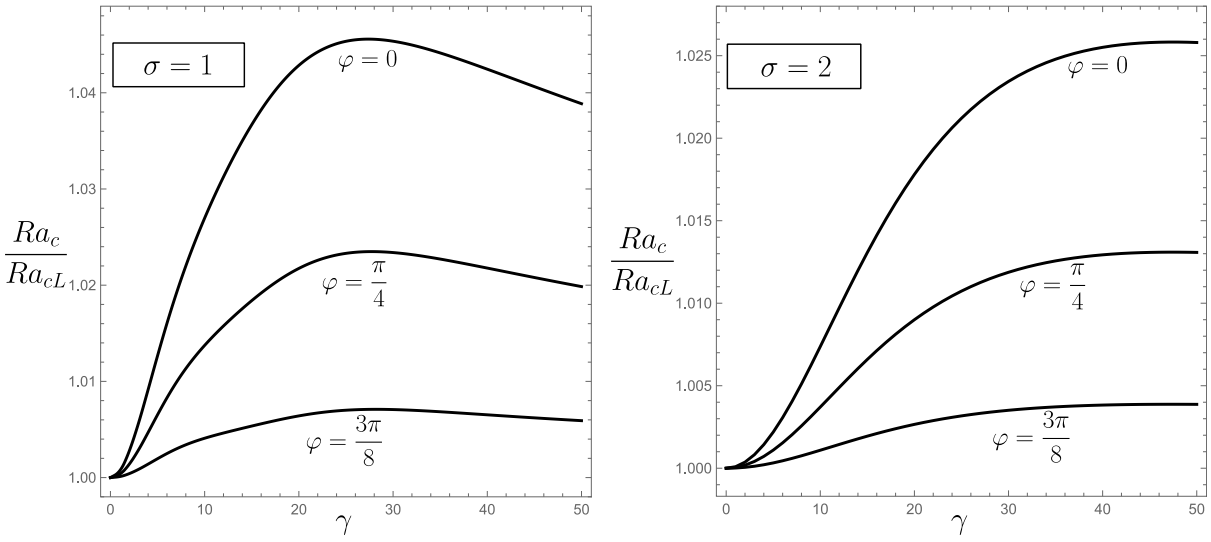

Fig. 9. Ratio between the critical values of Ra evaluated for oblique or transverse modes and those for longitudinal (L) modes versus γ for different values of $\sigma > 0$.

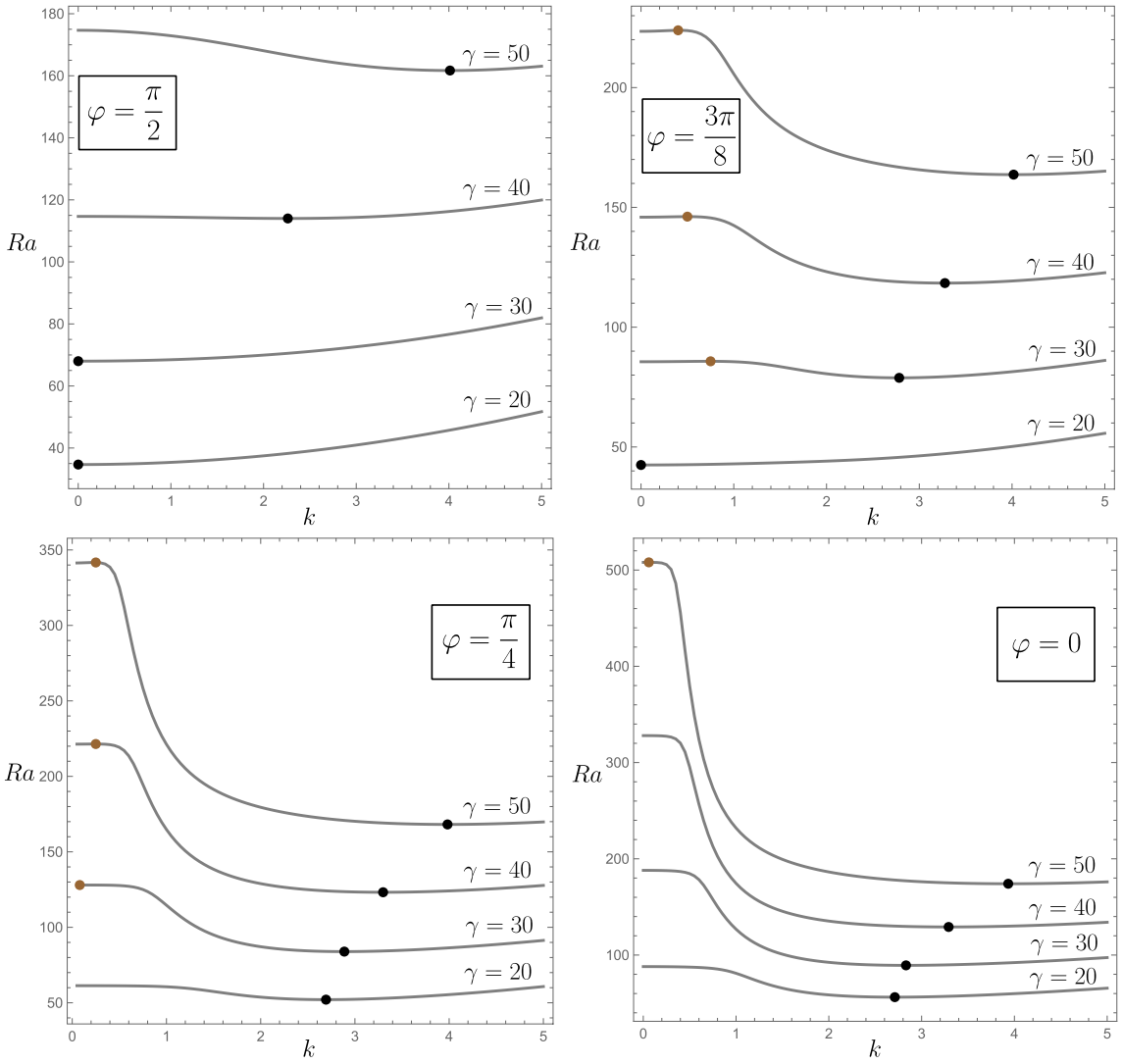

Fig. 10. Neutral stability curves in the (k, Ra) plane for $\sigma = -2$ and different values of γ and φ. The black dots denote the critical values (k_c, Ra_c), while the brown dots denote the local maxima of $Ra(k)$ with $k > 0$.

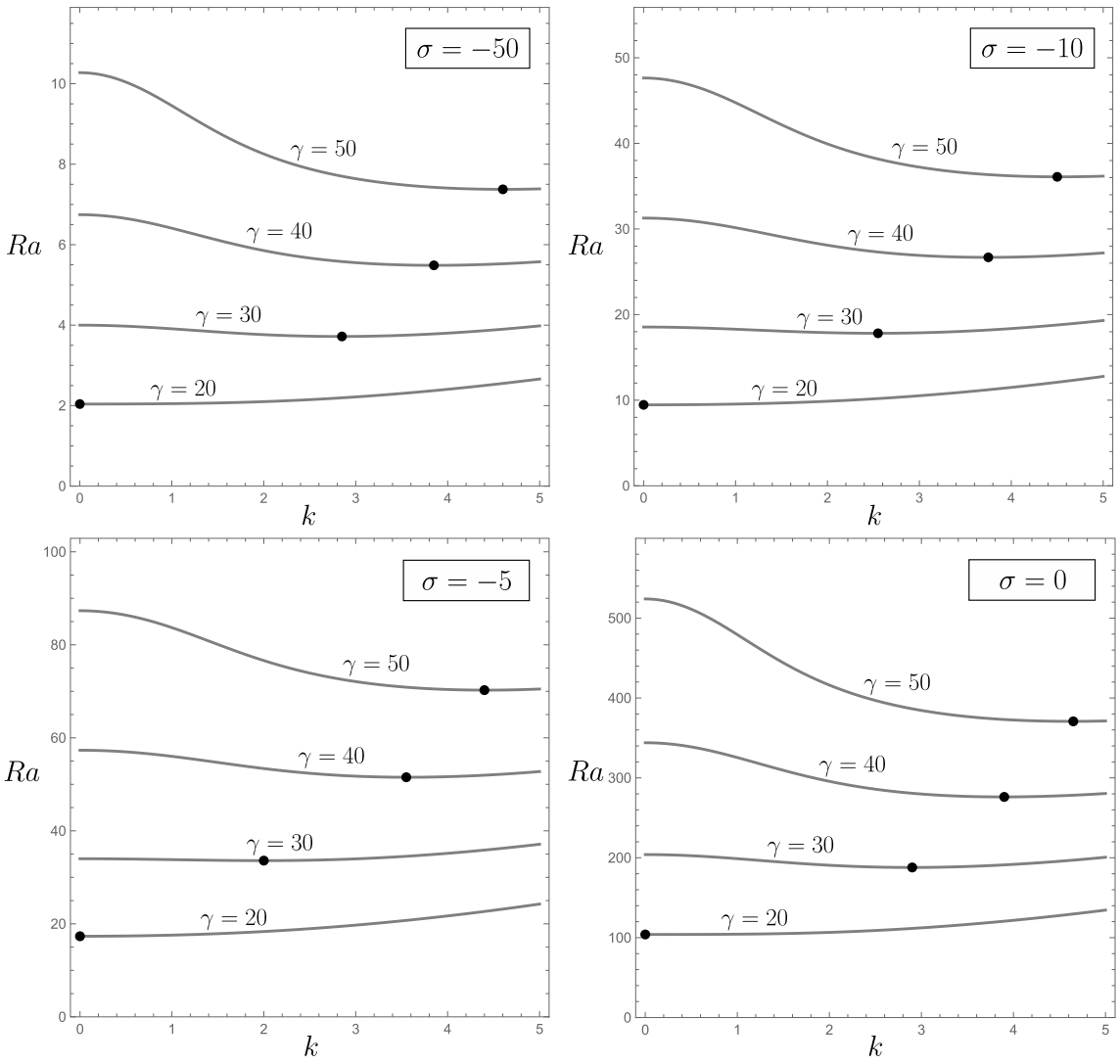

Fig. 11. Neutral stability curves in the (k, Ra) plane for longitudinal modes ($\varphi = \pi/2$) with different values of σ and γ. The black dots denote the critical values (k_c, Ra_c).

convection happens with $k_c = 0$, while the black colour line is relative to the case where the onset of convection happens with $k_c > 0$, the transition being at $\sigma = 0.634512$.

6.2. Perturbation modes with a nonzero γ

When $\gamma > 0$, the action of longitudinal, oblique or transverse modes is different, with the angle φ significantly affecting the neutral stability curves and the critical values $(k_c, Ra_c, \tilde{\omega}_c)$. A general feature is that, at neutral stability, $\tilde{\omega} \neq 0$ for every oblique and transverse modes, *i.e.*, when $0 \leq \varphi < \pi/2$.

Fig. 7 shows plots of Ra_c versus γ with different values of σ. The brown lines denote those cases where $Ra_c = Ra_0$ and $k_c = 0$, while the black lines are relative to cases where $k_c \neq 0$. The general trends shown by Fig. 7 reveal that Ra_c is a monotonic increasing function of both σ and γ. In fact, an increasing σ has a stabilising effect, as the heat flux q_2 supplied at the upper boundary increases, so that the thermal buoyancy becomes weaker and weaker. As already pointed out in Section 6.1, as well as in the comments on Fig. 4, the neutral stability curves in the domain $Ra > 0$ do not display an increasing trend for positive values of k close to 0 when σ exceeds the threshold defined by (31). Then, for σ larger than this threshold, the possibility that $k_c = 0$ is ruled out as shown in frame (b) of Fig. 7.

One may question whether the longitudinal modes considered in Fig. 7 are to be regarded as the most unstable. An argument showing that this is indeed the case is based on the plots reported in Figs. 8 and 9. Such figures display the ratio Ra_c/Ra_{cL} versus γ, where Ra_{cL} denotes the critical value of Ra evaluated for longitudinal modes. Several different values of σ have been considered for the evaluation of Ra_c/Ra_{cL} with three different inclination angles φ. For every (γ, σ) included in Figs. 8 and 9, the ratio Ra_c/Ra_{cL} turns out to be a decreasing function of φ suggesting that the longitudinal modes, associated with the maximum value, $\varphi = \pi/2$, are the most unstable perturbation modes for the basic state. This consideration means that the transition to linear instability occurs via longitudinal modes, even if there are parametric ranges where Ra_c for oblique or transverse modes is just a few percent larger than that for longitudinal modes. One may reckon that the cases envisaged in Fig. 9 show up such a feature. Both Fig. 8 and Fig. 9 confirm that the limit of Ra_c/Ra_{cL} when $\gamma \to 0$ is 1. In other words, one retrieves the behaviour in the limiting case $\gamma \to 0$, pointed out in Section 6.1, where the transition to linear instability is unaffected by the inclination angle φ, so that longitudinal, oblique and transverse modes are equivalent.

We already mentioned that the condition $Ra_2 < 0$ implies that k_c cannot be zero. However, the reverse is untrue, *i.e.*, when $Ra_2 > 0$ one may still have the minimum of function $Ra(k)$ for a nonzero wave

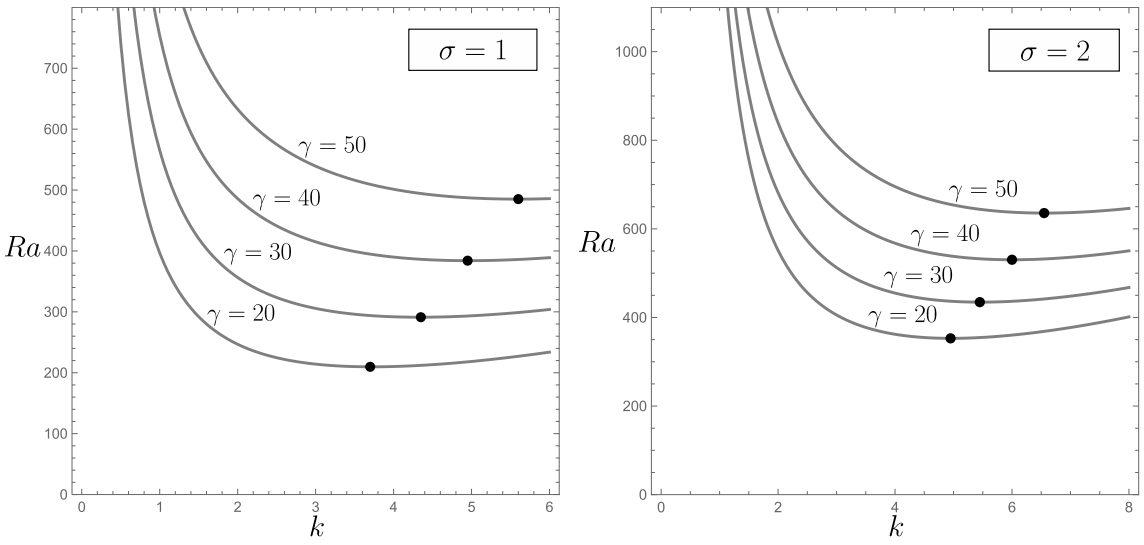

Fig. 12. Neutral stability curves in the (k, Ra) plane for longitudinal modes ($\varphi = \pi/2$) with different values of σ and γ. The black dots denote the critical values (k_c, Ra_c).

number. This finding is gathered by comparing Figs. 4 and 8 in the case $\sigma = -2$. For this case, Fig. 8 shows that $k_c > 0$ when γ exceeds a threshold which is approximately 24.0 for $\varphi = 3\pi/8$, 14.4 for $\varphi = \pi/4$ and 10.4 for $\varphi = 0$. On the other hand, Fig. 4 shows that, with $\sigma = -2$, $Ra_2 > 0$ for every γ when $\varphi = 3\pi/8$, and only within a limited range of γ when $\varphi = \pi/4$ or 0. The match between the information conveyed by Figs. 4 and 8 is found by examining the shape of the neutral stability curves displayed in Fig. 10. In this figure, the position of the critical point in the (k, Ra) plane is displayed in each case with a black dot. It is evidenced that there are cases where the neutral stability function $Ra(k)$ is increasing around $k = 0$, reaches a maximum (denoted with a brown dot) and then decreases reaching the minimum at $k = k_c > 0$. These are conditions where $Ra_2 > 0$ and, nonetheless, $k_c > 0$ with $Ra_c < Ra_0$. It is worth mentioning that, in every case, the increasing/decreasing trend of $Ra(k)$ around the brown dots, *i.e.* the local maxima, is barely perceptible in the plots of Fig. 10, for scale reasons, while it is utterly evident by inspecting the raw numerical data employed for such plots.

Having established, through the arguments presented above, that the transition to linear instability is driven by the longitudinal modes, hereafter, we will focus on such modes for the neutral stability curves and for the critical values of k and Ra. We emphasise again that the neutrally stable longitudinal modes are characterised by $\tilde{\omega} = 0$. Another important point regards the Ra_2 criterion for establishing whether $k_c = 0$ or $k_c > 0$. In fact, for longitudinal modes, $k_c = 0$ if and only if $Ra_2 > 0$. An illustration of the neutral stability curves for longitudinal modes ($\varphi = \pi/2$) in the (k, Ra) plane is provided in Figs. 11 and 12. While Fig. 11 is relative to cases where Ra at $k = 0$ is finite, with $\sigma \leq 0$, Fig. 12 displays neutral stability curves where $Ra \to \infty$ when $k \to 0$. Common features for all cases illustrated in these figures are that more stable conditions are found when either γ increases or σ increases. Strictly speaking, an increase in γ means that the streamwise temperature gradient in the basic flow gets larger, while increasing σ means reducing the destabilising action of the vertical temperature gradient. In particular, this circumstance suggests that extremely unstable flow conditions occur with $\sigma < 0$ when $|\sigma| \gg 1$. In order to analyse this asymptotic regime, let us assume that $\sigma \to -\infty$ with $Ra\,\sigma \sim \mathcal{O}(1)$ and $\gamma \sim \mathcal{O}(1)$. Evidently, taking the limit $\sigma \to -\infty$ with $Ra\,\sigma \sim \mathcal{O}(1)$ means that $Ra \to 0$. Thus, one can conveniently introduce a new parameter $\Lambda > 0$, defined as

$$\Lambda = -Ra\,\sigma. \tag{32}$$

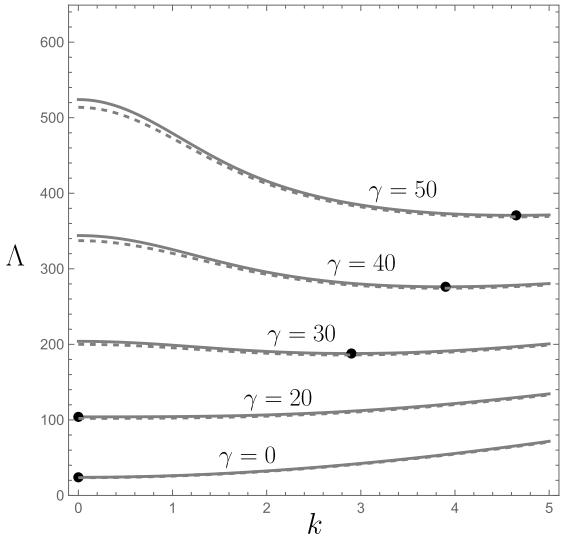

Fig. 13. Neutral stability curves in the (k, Λ) plane for longitudinal modes ($\varphi = \pi/2$) having different values of γ, with either $\sigma \to -\infty$ (solid lines) or $\sigma = -50$ (dashed lines). The black dots denote the critical values (k_c, Λ_c) with $\sigma \to -\infty$.

By taking the limit $\sigma \to -\infty$ with $\Lambda \sim \mathcal{O}(1)$, $\gamma \sim \mathcal{O}(1)$ and $\varphi = \pi/2$ in the eigenvalue problem (14), one obtains

$$\begin{aligned} &f'' - k^2 f + k\,h = 0, \\ &h'' - k^2 h - k\left[\frac{\gamma^2}{2}\,z(1-z) - \Lambda\,z\right] f = 0, \\ &z = 0, 1: \qquad f = 0, \quad h' = 0, \end{aligned} \tag{33}$$

where we also set $\eta = 0$ as we are interested in the neutral stability condition, and $\tilde{\omega} = 0$ as expected at neutral stability for longitudinal modes. The asymptotic eigenvalue problem (33) is solved numerically for a given γ, so that one can draw the neutral stability curves in the (k, Λ) plane. Fig. 13 shows a comparison between the neutral stability curves obtained by solving the eigenvalue problem (33) and those obtained from the data for $\sigma = -50$, already employed for the plots in Fig. 11. If the curves in Fig. 13 relative to $\sigma \to -\infty$ are identified as solid lines, those for $\sigma = -50$ are displayed as dashed lines. The comparison reveals a fair agreement, showing that one can approximately identify

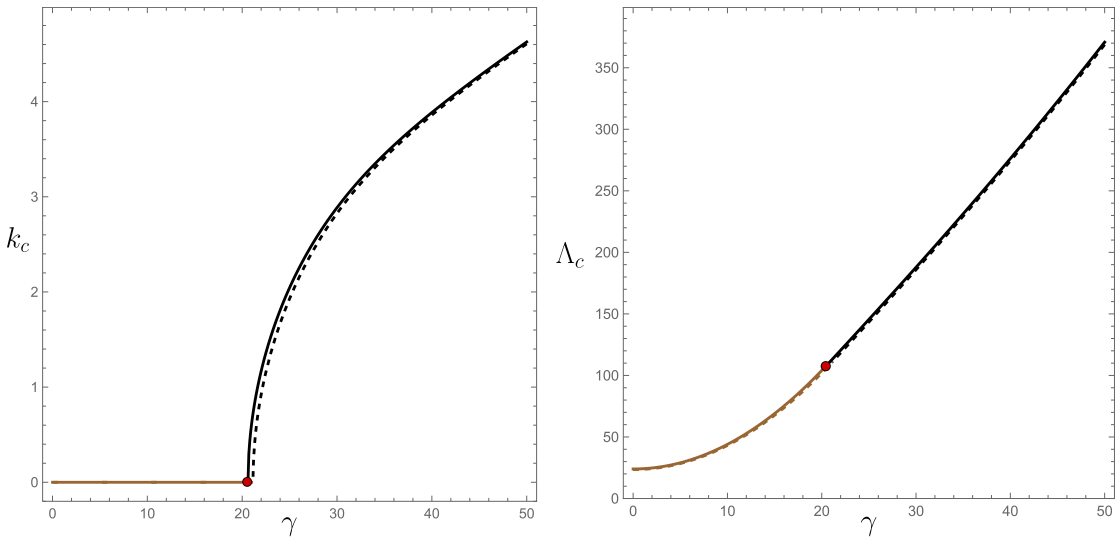

Fig. 14. Critical values of k and Λ versus γ for longitudinal modes ($\varphi = \pi/2$) with either $\sigma \to -\infty$ (solid lines) or $\sigma = -50$ (dashed lines). The brown lines are for the range where $k_c = 0$, while the black lines are relative to cases where $k_c > 0$.

Table 1
Critical values of k and Λ versus γ for the limiting case $\sigma \to -\infty$.

$\lvert\gamma\rvert$	k_c	Λ_c
0	0	24
5	0	29
10	0	44
20.6103	0	108.957
25	2.04516	145.500
30	2.88622	187.871
40	3.88578	276.187
50	4.62741	370.754

cases with $\sigma < -50$ with the asymptotic regime $\sigma \to -\infty$. One can also conclude that, in the limit $\sigma \to -\infty$, the critical Rayleigh number drops to zero meaning that the basic flow is unstable for every positive value of Ra. Such a result is a straightforward consequence of (32). The critical values of k and Λ are plotted versus γ in Fig. 14, where the solid lines are relative to $\sigma \to -\infty$, while the dashed lines are for $\sigma = -50$. This figure also identifies the range where $k_c = 0$ (in brown) and that where $k_c > 0$ (in black), the red dots label the transition point, for the limiting case with $\sigma \to -\infty$, occurring when

$$\gamma = 2\sqrt{\frac{10}{23}\left(\sqrt{89551} - 55\right)} \approx 20.6103, \tag{34}$$

as one can easily infer from the expression (27) of the coefficient Ra_2. Again, Fig. 14 shows the fair agreement between the data for $\sigma \to -\infty$ and those for $\sigma = -50$.

If Ra is the Rayleigh number based on the lower wall heat input, q_1, the parameter Λ defined by (32), is the Rayleigh number based on the upper wall heat removal rate, $-q_2$. This is a straightforward consequence of the definition (5). Thus, the limit $\sigma \to -\infty$ with $\gamma \sim \mathcal{O}(1)$ can be interpreted, from the physics viewpoint, as one where the lower boundary tends to be thermally insulated ($q_1 \to 0$) while the upper wall is uniformly cooled ($q_2 < 0$). This is a practically significant situation. We mention that such an interpretation of the limiting case $\sigma \to -\infty$ should be consistently stated by claiming that $\gamma < 0$, as one may infer from (7). However, the sign of γ has no effect on the numerical solution of the eigenvalue problem (33), as the latter just involves the square of γ. Therefore, beyond its significance as a mathematical asymptotic case, the limit $\sigma \to -\infty$ with $\gamma \sim \mathcal{O}(1)$ has a physical interest on its own. For this reason, we report the critical values k_c and Λ_c for some given $|\gamma|$ in Table 1. In fact, we expect no difference between the onset of instability in the case with adiabatic lower boundary and uniform cooling at the upper boundary and that in the case where we have uniform heating from below and an adiabatic upper boundary, namely the case where $\sigma = 0$ [10]. From the mathematical viewpoint this circumstance is a consequence of the symmetry defined in (28). This is the reason why the critical values of (k, Λ) reported in Table 1, for a given $|\gamma|$, coincide with the critical values of (k, Ra) evaluated for the case $\sigma = 0$.

7. Conclusions

A study of the onset of instability in a horizontal porous channel with uniform asymmetric wall heat fluxes at the horizontal boundaries has been carried out. A modal linear theory of perturbation dynamics has been employed to determine the neutral stability condition and the critical values of the wavenumber, k, and of the Rayleigh number, Ra. The basic stationary state whose instability is investigated involves a basic horizontal flow and a temperature gradient inclined to the vertical. The buoyancy force can trigger the instability for prescribed values of the pair (σ, γ), where the parameter σ is heat flux asymmetry ratio, while the parameter γ is the dimensionless horizontal temperature gradient in the basic state. Transition to instability is determined by the Rayleigh number. The most important results of the linear instability analysis presented in this paper are the following:

- The longitudinal modes, namely the wavelike modes directed perpendicularly to the basic flow direction, are the most unstable. In other words, the onset of instability is triggered by such modes.
- The parameter σ is stabilising. An increasing value of σ from $-\infty$ to $+\infty$ induces an increasing threshold Rayleigh number to linear instability, where such a threshold defines the condition of neutral stability.
- The parameter γ is also stabilising, where its growth from 0 to $+\infty$ determines an increasing critical Rayleigh number, Ra_c. The most unstable condition, for a fixed σ, is the limit $\gamma \to 0$ which physically means an infinite flow rate for the basic solution.
- The limiting case $\sigma \to -\infty$ is the most unstable, for every γ, and it implies a critical Rayleigh number to instability, Ra_c, equal to zero. This means that any basic flow with a positive Rayleigh number is unstable in this limiting case.
- The onset of the instability may be determined by infinite wavelength modes, *i.e.* modes with a zero critical wavenumber, k_c, under suitable parametric conditions determined by the pair (σ, γ). These conditions have been evaluated analytically through a series expansion in k for the solution of the stability eigenvalue problem.

The analysis carried out in this paper is the generalisation of the study published several years ago, regarding the special case where the wall heat fluxes are perfectly symmetric ($\sigma = 1$) [8]. With respect to that paper, the theoretical framework adopted in this study has an evident difference. In Barletta [8], the neutral stability curves in the (k, Ra) plane are parametrised by the Péclet number Pe, while in the present study we have used a parametrisation based on γ (for a prescribed σ). In practical terms, the parametrisation adopted in Barletta [8] is determined by the basic flow rate, while that adopted in this study is based on the horizontal temperature gradient for the basic state. Both approaches are perfectly legitimate, but the resulting neutral stability curves in the (k, Ra) plane are markedly different. Indeed, the γ-based approach adopted in this study leads to a mathematical neutral stability function $Ra(k)$ which is single-valued and defines the neutral stability curves in the (k, Ra) plane for every pair (σ, γ). On the other hand, the Pe-based approach leads to neutral stability curves in the (k, Ra) where $Ra(k)$ is not single-valued and, hence, does not define a neutral stability function [8]. In fact, Barletta [8] found neutral stability curves in the (k, Ra) plane which, for a decreasing Pe, tend to assume a closed loop shape. Such closed loops gradually shrink to a point and eventually disappear when Pe attains a minimum below which no linear instability arises [8]. It is not surprising that different parametrisations lead to seemingly different graphical representations of the same neutral stability condition. The question on which is the best approach to be followed or, at least, the most effective one in the discussion of the instability onset conditions has possibly no good answer. Every different parametrisation of a given stability problem focusses on the role played by different physical quantities which, ultimately, reflect the experimental conditions under which the flow dynamics is controlled. In principle, a given experimental apparatus can be designed to fix either the horizontal temperature gradient (the γ-based approach) or the flow rate (the Pe-based approach) in the basic state.

We finally mention that this study is confined to linear analysis and position nonlinear stability analysis or direct numerical simulation (DNS) as the most critical next steps for future research to fully unravel the physics in the supercritical regime.

CRediT authorship contribution statement

A. Barletta: Writing – review & editing, Writing – original draft, Visualization, Validation, Methodology, Investigation, Funding acquisition, Formal analysis, Conceptualization. **M. Celli:** Writing – review & editing, Writing – original draft, Visualization, Validation, Methodology, Investigation, Funding acquisition, Formal analysis, Conceptualization. **P.V. Brandão:** Writing – review & editing, Writing – original draft, Visualization, Validation, Methodology, Investigation, Funding acquisition, Formal analysis, Conceptualization.

Declaration of competing interest

The authors declare the following financial interests/personal relationships which may be considered as potential competing interests: All authors report financial support was provided by Alma Mater Studiorum Universitá di Bologna. All authors declare that they have no known competing financial interests or personal relationships that could have appeared to influence the work reported in this paper.

Acknowledgements

The work by Antonio Barletta, Michele Celli and Pedro Vayssière Brandão was supported by Alma Mater Studiorum Università di Bologna, grant number RFO-2024.

Data availability

No data was used for the research described in the article.

References

[1] D.A. Nield, A. Bejan, Convection in Porous Media, fifth ed., Springer, New York, 2017.
[2] M. Prats, The effect of horizontal fluid flow on thermally induced convection currents in porous mediums, J. Geophys. Res. 71 (1966) 4835–4838.
[3] F. Dufour, M.-C. Neel, Numerical study of instability in a horizontal porous channel with bottom heating and forced horizontal flow, Phys. Fluids 10 (1998) 2198–2207.
[4] T.J. Chung, J.H. Park, C.K. Choi, D.-Y. Yoon, The onset of vortex instability in laminar forced convection flow through a horizontal porous channel, Int. J. Heat Mass Transfer 45 (2002) 3061–3064.
[5] M.N. Ouarzazi, F. Mejni, A. Delache, G. Labrosse, Nonlinear global modes in inhomogeneous mixed convection flows in porous media, J. Fluid Mech. 595 (2008) 367–377.
[6] A. Delache, M. Ouarzazi, Weakly nonlinear interaction of mixed convection patterns in porous media heated from below, Int. J. Therm. Sci. 47 (2008) 709–722.
[7] T.J. Chung, C.K. Choi, D.-Y. Yoon, M.C. Kim, Onset of buoyancy-driven motion with laminar forced convection flows in a horizontal porous channel, Int. J. Heat Mass Transfer 53 (2010) 5139–5146.
[8] A. Barletta, Thermal instability in a horizontal porous channel with horizontal through flow and symmetric wall heat fluxes, Transp. Porous Media 92 (2012) 419–437.
[9] A. Barletta, M. Celli, A.V. Kuznetsov, Convective instability of the Darcy flow in a horizontal layer with symmetric wall heat fluxes and local thermal nonequilibrium, ASME J. Heat Transf. 136 (2014) 012601.
[10] L.A. Sphaier, A. Barletta, Unstable mixed convection in a heated horizontal porous channel, Int. J. Therm. Sci. 78 (2014) 77–89.
[11] R. Dubey, P.V.S.N. Murthy, The onset of convective instability of horizontal throughflow in a porous layer with inclined thermal and solutal gradients, Phys. Fluids 30 (2018) 074104.
[12] A. Barletta, D.A.S. Rees, Unstable mixed convection flow in a horizontal porous channel with uniform wall heat flux, Transp. Porous Media 129 (2019) 385–402.
[13] A. Barletta, M. Celli, P.V. Brandão, S. Lazzari, E. Ghedini, Linearly unstable forced and free flow in an anisotropic porous channel, Int. J. Heat Mass Transfer 235 (2024) 126155.
[14] R. Dubey, R. Chetteti, The influence of thermal dispersion on the initiation of convective instability in Prats flow through a low permeability porous medium, Phys. Fluids 36 (2024) 014104.
[15] B. Straughan, The Energy Method, Stability, and Nonlinear Convection, Springer, 2013.
[16] A. Barletta, Routes To Absolute Instability in Porous Media, Springer, 2019.
[17] B. Buonomo, A. di Pasqua, O. Manca, S. Nardini, Evaluation of thermal and fluid dynamic performance parameters in aluminum foam compact heat exchangers, Appl. Therm. Eng. 176 (2020) 115456.
[18] V. Bianco, B. Buonomo, A. di Pasqua, O. Manca, Heat transfer enhancement of laminar impinging slot jets by nanofluids and metal foams, Therm. Sci. Eng. Prog. 22 (2021) 100860.
[19] W.L. Lin, T.F. Lin, Experimental study of unstable mixed convection of air in a bottom heated horizontal rectangular duct, Int. J. Heat Mass Transfer 39 (1996) 1649–1663.
[20] M.Y. Chang, C.H. Yu, T.F. Lin, Changes of longitudinal vortex roll structure in a mixed convective air flow through a horizontal plane channel: an experimental study, Int. J. Heat Mass Transfer 40 (1997) 347–363.
[21] M.Y. Chang, T.F. Lin, Experimental study of aspect ratio effects on longitudinal vortex flow in mixed convection of air in a horizontal rectangular duct, Int. J. Heat Mass Transfer 41 (1998) 719–733.
[22] C. Tian, J. Wang, X. Cao, C. Yan, A.A. Ala, Experimental study on mixed convection in an asymmetrically heated, inclined, narrow, rectangular channel, Int. J. Heat Mass Transfer 116 (2018) 1074–1084.
[23] A. Barletta, P.V. Brandão, M. Celli, An alternative numerical solution for the Orr-Sommerfeld problem, Eur. Phys. J. Plus 139 (2024) 102.
[24] A. Barletta, G. Mulone, Energy method and stability of shear flows: an elementary tutorial, Eur. Phys. J. Plus 139 (2024) 906.
[25] K.R. Rajagopal, M. Ruzicka, A.R. Srinivasa, On the Oberbeck-Boussinesq approximation, Math. Models Methods Appl. Sci. 6 (1996) 1157–1167.
[26] A. Barletta, The Boussinesq approximation for buoyant flows, Mech. Res. Commun. 124 (2022) 103939.
[27] M. Combarnous, Convection naturelle et convection mixte dans une couche poreuse horizontale, Rev. Générale de Therm. 9 (1970) 1335–1355.
[28] A. Delache, M.N. Ouarzazi, M. Combarnous, Spatio-temporal stability analysis of mixed convection flows in porous media heated from below: Comparison with experiments, Int. J. Heat Mass Transfer 50 (2007) 1485–1499.

[29] I. Kurtbas, N. Celik, Experimental investigation of forced and mixed convection heat transfer in a foam-filled horizontal rectangular channel, Int. J. Heat Mass Transfer 52 (2009) 1313–1325.
[30] P.V. Brandão, A. Barletta, M. Celli, L.S. d. B. Alves, D.A.S. Rees, On the stability of the isoflux Darcy-Bénard problem with a generalised basic state, Int. J. Heat Mass Transfer 177 (2021) 121538.
[31] M. Turkyilmazoglu, A.A. Siddiqui, The instability onset of generalized isoflux mean flow using Brinkman-Darcy-Bénard model in a fluid saturated porous channel, Int. J. Therm. Sci. 188 (2023) 108249.
[32] Wolfram Research, Inc., Mathematica, Version 14.2, 2024, https://www.wolfram.com/mathematica.
[33] R.J. Buretta, A.S. Berman, Convective heat transfer in a liquid saturated porous layer, ASME J. Appl. Mech. 43 (1976) 249–253.